Automatic wave-equation migration velocity analysis

Biondo Biondi

ABSTRACT

I present a general framework to formalize a wide class of wave-equation velocity-estimation methods that search for the velocity function that optimally focuses the migrated image. Two well-known methods, the Differential Semblance Optimization (DSO) method and the Wave-Equation Migration Velocity Analysis (WEMVA), are particular instances of velocity-estimation methods that can be formalized in this framework. I define a WEMVA-like algorithm that exploits the potential of residual migration for velocity estimation but does not require the picking of residual-migration parameters. This result enables the derivation of a closed-form expression for the gradient of the objective function, making possible to use quasi-Newton methods to solve the optimization problem. I use a simple synthetic example to illustrate some of the characteristics of the method, and to evaluate its potential as a velocity estimation method.

INTRODUCTION

Tomographic velocity estimation based on wave-equation operators has the potential of improving the imaging in areas where wavefield-continuation migration is needed. Among the most promising methods to update velocity using wave-equation operators are the ones that formulate the velocity estimation problem as a maximization of the image focusing in the migrated domain. Two important examples of this approach are the Wave-Equation Migration Velocity Analysis (WEMVA) method (Biondi and Sava, 1999; Sava and Biondi, 2004a,b; Sava, 2004) and the Differential Semblance Optimization (DSO) (Symes and Carazzone, 1991; Shen, 2004; Shen et al., 2005b). However, each iteration of wave-equation velocity updating is computationally expensive and convergence is often slow. Practical applications are still rare and small in scale (Sava, 2004; Shen et al., 2005a; Albertin et al., 2006). The goal of this paper is to present a general framework for formalizing wave-equation velocity estimation methods that comprise both the DSO and the WEMVA methods. I follow the idea presented by Sava and Symes (2002), but I further generalize and develop it to devise a velocity estimation method that should benefit from the relative advantages of both DSO and WEMVA methods and overcome some of their shortcomings.

The WEMVA method has the practical disadvantage over the DSO method that it includes a picking step of the residual-migration parameters ($\mathbf{\Delta}\rho$), and thus it is less

amenable to automatic implementations. Furthermore, as I will discuss in more detail in the next section, it does not lend itself to the application of efficient quasi-Newton optimization methods that may speed up convergence (Shen, 2004; Maharramov and Albertin, 2007). On the other hand, the WEMVA method has the fundamental advantage of harnessing the power of residual migration for the velocity estimation process. Residual migration has the potential of extracting velocity information from the image focusing, or lack thereof, along the midpoint directions as well as the offset/angle directions. This can be useful, when the velocity resolution afforded by analyzing common image gathers is low because of poor angular coverage (e. g. subsalt). Sava et al. (2005) show a promising example of the application of residual migration to estimate velocity from the focusing of diffracted events.

Another, and more "technical", reason for relying on residual migration is that the wave-equation tomographic operators used to invert image perturbations (Biondi and Sava, 1999; Shen, 2004) are derived as the first-order Born linearization of wavefield-continuation migration. Therefore, the image perturbations (data residuals in inversion terminology) created by residual migration are more consistent with the wave-equation tomographic operator (modeling operator) than the image perturbations created by either applying residual moveout (RMO) or DSO. For example, in presence of a uniform velocity perturbation the wave-equation tomographic operator predicts a bulk shift of the migrated events at all reflection angles in migrated angle-domain common image gathers. This bulk shift of the whole events is inconsistent with the image perturbations inverted when applying the DSO method; these image perturbations are different from zero only for wide aperture angles where there is substantial differential shift between the image at adjacent angles.

The general framework that I introduce in this paper allows the formulation of a method to perform wave-equation MVA that does not include a picking step of the residual-migration parameters ($\mathbf{\Delta}\rho$). The vector of residual-migration parameters $\mathbf{\Delta}\rho$ that is needed by residual migration is estimated by computing the gradient direction of an auxiliary optimization problem formulated as a function of $\mathbf{\Delta}\rho$. This explicit evaluation of $\mathbf{\Delta}\rho$ also enables the derivations of a closed-form expression for the gradient of the primary objective function, which now can be minimized by efficient quasi-Newton algorithms. Because of the ability of the proposed method to avoid the picking step, I will call it Automatic WEMVA, or for short, AWEMVA.

The new general framework should also enable to easily substitute in the AWEMVA procedure other useful residual-focusing operators, such as a multi-parameter residual-migration operators, for the single-parameter residual migration I use in this paper. This improvement should help the convergence at the later stages of the estimation process, when the spatial variability of the residual velocity errors causes the migrated gathers to have complex moveout as a function of the aperture angle(s). Other possible research directions that are made possible by the general framework is the tailoring of the objective function to specific velocity problems, such as the ones related to shallow-velocity anomalies or velocity estimation in presence of shadow zones.

GENERAL FRAMEWORK FOR WAVE-EQUATION MVA

A general formulation of the velocity estimation problem, that comprises both the DSO inversion as well as the WEMVA method, is the minimization of the following objective function:

$$J_{\mathbf{s}} = \frac{1}{2} \left\| \mathbf{R} - \mathbf{F}\left(\mathbf{R}\left(\mathbf{s}\right)\right) \right\|_2 , \tag{1}$$

where $\mathbf{R}$ is the prestack image obtained by wavefield continuation migration, $\mathbf{s}$ is the slowness function, and $\mathbf{F}$ is a differential residual-focusing operator. For example, we could define the differential residual-focusing operator using the DSO operator, $\mathbf{D}$, as:

$$\mathbf{F}\left(\mathbf{R}\right) = \left(\mathbf{I} - \mathbf{D}\right)\mathbf{R}, \tag{2}$$

where $\mathbf{I}$ is the identity operator. The DSO operator can be either applied in the subsurface-offset domain or in the angle domain.

In the particular case of DSO, the objective function in equation 1 simplifies into the following well-known form (Shen, 2004):

$$J_{\mathbf{s}} = \frac{1}{2} \left\| \mathbf{DR}\left(\mathbf{s}\right) \right\|_2 . \tag{3}$$

The more general idea behind the objective function in equation 1 is that the optimally-focused image is achieved when no more residual focusing is possible, and thus the application of the residual-focusing operator is equivalent to the application of an identity operator. In the particular example of DSO (equations 2 and 3), the result of applying DSO to an image is null when all the events in the image are either focused at zero subsurface offset (subsurface-offset domain image), or they are aligned in the angle domain (angle-domain image).

In this paper I am mostly concerned with the choice of a differential residual-focusing operator that takes advantage of the potential of residual migration to improve the focusing of the image. Sava and Biondi (2004a) introduced a differential residual-migration operator based on residual prestack Stolt migration (Sava, 2003). I am using a similar differential residual-migration operator (presented in the Appendix) that is not based on Stolt migration but on the derivation of residual moveout in the angle domain introduced by Biondi and Symes (2004).

The residual migration introduced in the Appendix is less accurate than the one introduced by (Sava, 2003) for large velocity errors because it is based on a stationary raypath linearization. However, the differential residual migration I introduce should be practically equivalent to the one introduced by Sava and Biondi (2004a) but have substantial efficiency advantages. It can be directly applied to the 3D prestack image transformed into the angle domain, and thus does not require a large transpose of the prestack image cube, which can be an expensive and cumbersome operation. Furthermore, the residual migration introduced here is more amenable to potentially useful generalizations that use several parameters to describe the residual moveout

across aperture angles. Other residual-focusing operators could be used as well; for example, in one of the numerical test shown in the next section I use the residual-moveout operator introduced by Biondi and Symes (2004).

I use differential residual-focusing operator, and not a conventional "finite" residual-focusing operator because they are consistent with the first-order Born linearization of wavefield-continuation migration, as amply discussed by Sava and Biondi (2004a) and Sava (2004). Such differential residual-focusing operators can be generally defined as

$$\mathbf{F}\left(\mathbf{R}\right) = \left(\mathbf{I} + \mathbf{K}\left[\mathbf{\Delta}\rho\right]\right)\mathbf{R}, \tag{4}$$

where the linear operator $\mathbf{K}$ applies different phase rotations to the image for different reflection angles and geological dips. The operator is a function of a vector of residual-focusing parameters $\mathbf{\Delta}\rho$ that is defined in the $(z, \mathbf{x})$ of the spatial coordinates depth, z, and horizontal location, $\mathbf{x}$.

When the input image is fixed the differential residual-focusing operators are also linear functions of the vector $\mathbf{\Delta}\rho$. It is thus useful to introduce the following notation to represent the linear operator $\mathbf{M}$ that, for a fixed image $\mathbf{R}$, has the domain defined in the space of the vectors $\mathbf{\Delta}\rho$ and the range defined in the image space,

$$\mathbf{M}\left[\mathbf{R}\right] = \frac{\partial \mathbf{K}\left[\mathbf{\Delta}\rho\right]\mathbf{R}}{\partial \mathbf{\Delta}\rho}. \tag{5}$$

One of the main obstacles to the application of WEMVA as defined by Sava and Biondi (2004a) and Sava (2004) is the estimation of the vector of residual-focusing parameters $\mathbf{\Delta}\rho$ by an automatic, efficient, and robust procedure. I propose to estimate $\mathbf{\Delta}\rho$ by (approximately) solving an auxiliary optimization problem defined as the minimization of the following objective function

$$\begin{aligned} J_{\mathbf{\Delta}\rho} &= \frac{1}{2}\epsilon_{\mathbf{D}} \left\|\mathbf{DF}\left(\mathbf{\Delta}\rho, \mathbf{R}\left(\mathbf{s}\right)\right)\right\|_2 - \frac{1}{2}\epsilon_{\mathbf{S}} \left\|\mathbf{SF}\left(\mathbf{\Delta}\rho, \mathbf{R}\left(\mathbf{s}\right)\right)\right\|_2 \\ &= \frac{1}{2}\epsilon_{\mathbf{D}} \left\|\mathbf{DR} + \mathbf{DM}\left[\mathbf{R}\right]\mathbf{\Delta}\rho\right\|_2 - \frac{1}{2}\epsilon_{\mathbf{S}} \left\|\mathbf{DR} + \mathbf{SM}\left[\mathbf{R}\right]\mathbf{\Delta}\rho\right\|_2, \end{aligned} \tag{6}$$

where $\mathbf{S}$ is a "stacking" operator that actually stacks over reflection angles when the prestack image is defined in the angle domain, or extracts the zero-offset cube when the prestack image is defined in the subsurface-offset domain. The weights $\epsilon_{\mathbf{D}}$ and $\epsilon_{\mathbf{S}}$ provide a trade-off between a minimization of the differential-semblance criterion, which has appealing properties for global convergence, and a maximization of the stacking power, which has attractive high-resolution characteristics close to the solution.

It would be relatively straightforward and inexpensive to find the minimum of the objective function in equation 6 by an iterative optimization scheme. However, to provide a closed-form representation of the gradient of the main objective function (equation 1), I will use, as an estimate of the optimal $\mathbf{\Delta}\rho$, the gradient of the objective

function in equation 6, evaluated at $\mathbf{\Delta}\rho = 0$, and smoothed by a simple smoothing operator $\mathbf{G}$; that is:

$$\widehat{\mathbf{\Delta}\rho} = \mathbf{G}\nabla J_{\mathbf{\Delta}\rho} = \mathbf{G}\mathbf{M}'\left[\mathbf{R}\right]\left(-\epsilon_{\mathbf{D}}\mathbf{D}'\mathbf{D} + \epsilon_{\mathbf{S}}\mathbf{S}'\mathbf{S}\right)\mathbf{R} = \mathbf{G}\mathbf{M}'\left[\mathbf{R}\right]\mathbf{C}\mathbf{R}, \tag{7}$$

where, to simplify the expressions that describe the development that follows, I introduce the following identity

$$\mathbf{C} = -\epsilon_{\mathbf{D}}\mathbf{D}'\mathbf{D} + \epsilon_{\mathbf{S}}\mathbf{S}'\mathbf{S}. \tag{8}$$

WEMVA approximation of the gradient

To solve the optimization problem formalized in equation 1, we need to compute the gradient of the objective function with respect to the slowness model $\mathbf{s}$. According to the "classical" WEMVA solution (Sava and Biondi, 2004a), the gradient is evaluated by fixing both the focusing-parameters vector $\mathbf{\Delta}\rho$ and the image to which the residual focusing operator is applied; that is, by ignoring their dependence on $\mathbf{s}$ and assuming that the image is the background image $\mathbf{R_0}$ obtained by migrating the data with the current best-estimate of the slowness function, and that the vector $\mathbf{\Delta}\rho$ is either picked or evaluated by equation 7.

With these assumptions, the residual-focusing operator is

$$\mathbf{F}_0 = \mathbf{F}\left(\mathbf{R_0}\right) = \mathbf{R_0} + \mathbf{K}\left[\widehat{\mathbf{\Delta}\rho}\right]\mathbf{R_0}, \tag{9}$$

and the objective function can be written as:

$$\begin{aligned} J_{\mathbf{s}} &= \frac{1}{2}\left\|\mathbf{R} - \left(\mathbf{R_0} + \mathbf{K}\left[\widehat{\mathbf{\Delta}\rho}\right]\mathbf{R_0}\right)\right\|_2 \\ &= \frac{1}{2}\left\langle \mathbf{R} - \left(\mathbf{R_0} + \mathbf{K}\left[\widehat{\mathbf{\Delta}\rho}\right]\mathbf{R_0}\right), \mathbf{R} - \left(\mathbf{R_0} + \mathbf{K}\left[\widehat{\mathbf{\Delta}\rho}\right]\mathbf{R_0}\right)\right\rangle, \end{aligned} \tag{10}$$

$$\tag{11}$$

where with the notation $\langle \mathbf{x}, \mathbf{y} \rangle$ I indicate the inner product of the vectors $\mathbf{x}$ and $\mathbf{y}$.

The perturbation $\delta J_{\mathbf{s}}$ in the objective function caused by a perturbation in the slowness model $\delta\mathbf{s}$ is:

$$\delta J_{\mathbf{s}} = \left\langle \mathbf{R} - \left(\mathbf{R_0} + \mathbf{K}\left[\widehat{\mathbf{\Delta}\rho}\right]\mathbf{R_0}\right), \delta\mathbf{R}\right\rangle = \left\langle \mathbf{R} - \left(\mathbf{R_0} + \mathbf{K}\left[\widehat{\mathbf{\Delta}\rho}\right]\mathbf{R_0}\right), \mathbf{L}\delta\mathbf{s}\right\rangle, \tag{12}$$

where $\mathbf{L}$ is the wave-equation tomographic operator relating perturbations in slowness to perturbations in the image ($\delta\mathbf{R} = \mathbf{L}\delta\mathbf{s}$) that was introduced by Biondi and Sava (1999) for source-receiver migration, and by Shen (2004) for shot-profile migration.

The gradient of the objective function is therefore

$$\nabla J_{\mathbf{s}} = \mathbf{L}'\left(\mathbf{R} - \left(\mathbf{R_0} + \mathbf{K}\left[\widehat{\mathbf{\Delta}\rho}\right]\mathbf{R_0}\right)\right). \tag{13}$$

When the gradient is evaluated for $\mathbf{R} = \mathbf{R_0}$ it becomes

$$\nabla J_{\mathbf{s}}|_{\mathbf{R}=\mathbf{R_0}} = -\mathbf{L}'\mathbf{K}\left[\widehat{\mathbf{\Delta}\rho}\right]\mathbf{R_0}, \tag{14}$$

as presented by Sava (2004).

Another way of reaching the same result is to assume linear perturbations in the image and substitue $\mathbf{R} = \mathbf{R_0} + \mathbf{L}\delta\mathbf{s}$ in equation 10. I can then derive the quadratic objective function

$$J_{\mathbf{s}} = \frac{1}{2}\left\|\mathbf{L}\delta\mathbf{s} - \mathbf{K}\left[\widehat{\mathbf{\Delta}\rho}\right]\mathbf{R_0}\right\|_2, \tag{15}$$

that has the gradient expressed in equation 14.

Complete gradient

As discussed in the previous section, the gradient provided by the WEMVA method is an approximation of the full gradient of the objective function with respect to slowness. It is based on the assumption that both inputs to the residual focusing operator are independent from the slowness. This approximation may be inconsequential if the velocity estimation problem is solved by nesting several linearized iterations within an outer loop of non-linear iterations. Following this approach, a background velocity model is defined at each non-linear iteration, and the quadratic objective function in equation 15 is optimized with several steps of a conjugate gradient algorithm.

Shen (2004) and Maharramov and Albertin (2007) report success with a different optimization strategy when minimizing the DSO objective function in equation 3. He used a quasi-Newton optimization method (limited memory BFGS) that builds up information on the Hessian with iterations. Quasi-Newton methods can be more efficient when solving an ill-conditioned non-quadratic optimization problem; however, they are sensitive to approximations in the gradient computation. It is thus useful to derive a procedure to compute the gradient that overcomes the approximations discussed above. On the other hand, one disadvantage of employing a quasi-Newton method is that at each iteration we need to recompute the background wavefields that are needed to evaluate $\mathbf{L}$ and its adjoint. This requirement of updating the background wavefields more than doubles the computational cost of the quasi-Newton iterations over the cost of the linearized iterations needed to solve the quadratic objective function defined in equation 15.

If the residual migration operator is applied to the current image $\mathbf{R}$, the objective function in equation 1 becomes

$$J_{\mathbf{s}} = \frac{1}{2}\left\|-\mathbf{K}\left[\mathbf{\Delta}\rho\right]\mathbf{R}\right\|_2 = \frac{1}{2}\left\langle-\mathbf{K}\left[\mathbf{\Delta}\rho\right]\mathbf{R}, -\mathbf{K}\left[\mathbf{\Delta}\rho\right]\mathbf{R}\right\rangle. \tag{16}$$

If the dependence of both $\mathbf{R}$ and $\mathbf{\Delta}\rho$ from the slowness function are taken into account, the perturbations in $J_{\mathbf{s}}$ caused by image perturbations $\delta\mathbf{R}$ are formally expressed as

$$\delta J_{\mathbf{s}} = \left\langle-\mathbf{K}\left[\mathbf{\Delta}\rho\right]\mathbf{R}, -\mathbf{K}\left[\mathbf{\Delta}\rho\right]\delta\mathbf{R} - \mathbf{K}\left[\mathbf{\Delta}\rho + \delta\mathbf{\Delta}\rho\left(\delta\mathbf{R}\right)\right]\mathbf{R}\right\rangle \tag{17}$$

If the estimate $\widehat{\mathbf{\Delta}\rho}$ for the optimal perturbation in the focusing parameters vectors expressed in equation 7 is used, then equation 17 becomes

$$\begin{aligned}\delta J_{\mathbf{s}} &= \langle -\mathbf{K}\left[\mathbf{\Delta}\rho\right]\mathbf{R}, -\mathbf{K}\left[\mathbf{\Delta}\rho\right]\delta\mathbf{R} - \mathbf{K}\left[\mathbf{\Delta}\rho + \mathbf{G}\mathbf{M}'\left[\mathbf{R}\right]\mathbf{C}\delta\mathbf{R}\right]\mathbf{R}\rangle \\ &= \langle -\mathbf{K}\left[\mathbf{\Delta}\rho\right]\mathbf{R}, -\mathbf{K}\left[\mathbf{\Delta}\rho\right]\delta\mathbf{R} - \mathbf{M}\left[\mathbf{R}\right]\mathbf{G}\mathbf{M}'\left[\mathbf{R}\right]\mathbf{C}\delta\mathbf{R}\rangle \\ &= \langle -\mathbf{K}\left[\mathbf{\Delta}\rho\right]\mathbf{R}, -\left(\mathbf{K}\left[\mathbf{\Delta}\rho\right] + \mathbf{M}\left[\mathbf{R}\right]\mathbf{G}\mathbf{M}'\left[\mathbf{R}\right]\mathbf{C}\right)\delta\mathbf{R}\rangle\,,\end{aligned} \tag{18}$$

where $\mathbf{M}$ is defined in equation 5.

The objective-function perturbations caused by slowness perturbations are written as:

$$\delta J_{\mathbf{s}} = \langle -\mathbf{K}\left[\mathbf{\Delta}\rho\right]\mathbf{R}, -\left(\mathbf{K}\left[\mathbf{\Delta}\rho\right] + \mathbf{M}\left[\mathbf{R}\right]\mathbf{G}\mathbf{M}'\left[\mathbf{R}\right]\mathbf{C}\right)\mathbf{L}\delta\mathbf{s}\rangle \tag{19}$$

and the gradient becomes

$$\nabla J_{\mathbf{s}} = \mathbf{L}'\left(\mathbf{K}'\left[\mathbf{\Delta}\rho\right] + \mathbf{C}'\mathbf{M}\left[\mathbf{R}\right]\mathbf{G}'\mathbf{M}'\left[\mathbf{R}\right]\right)\mathbf{K}\left[\mathbf{\Delta}\rho\right]\mathbf{R}. \tag{20}$$

that can be rewritten as the sum of two terms; that is,

$$\nabla J_{\mathbf{s}} = \mathbf{L}'\mathbf{K}'\left[\mathbf{\Delta}\rho\right]\mathbf{K}\left[\mathbf{\Delta}\rho\right]\mathbf{R} + \mathbf{L}'\mathbf{C}'\mathbf{M}\left[\mathbf{R}\right]\mathbf{G}'\mathbf{M}'\left[\mathbf{R}\right]\mathbf{K}\left[\mathbf{\Delta}\rho\right]\mathbf{R}. \tag{21}$$

The first term in the gradient in 21 is related to the image perturbations that are directly caused by perturbations in slowness. The second term is related to the image perturbations caused indirectly through perturbations in the optimal estimate of residual-focusing parameters $\widehat{\mathbf{\Delta}\rho}$. When the residual focusing operator is not defined in parametric form but it is fixed, as for the important case of DSO, the second term vanishes, and we get the well-known expression for the gradient of the objective function in equation 3 (Shen, 2004):

$$\nabla J_{\mathbf{s}} = \mathbf{L}'\mathbf{D}'\mathbf{D}\mathbf{R}. \tag{22}$$

Notice that the application of the adjoint operator of the differential residual-focusing operator in both the first term of the gradient in equation 21 and in the DSO gradient in equation 22 removes the phase rotation from the image that is back-projected by the wave-equation tomographic operator. Intuitively, this lack of phase information in the image perturbations may slow the convergence towards a better focused image. The numerical tests I show in the next section are too preliminary to shed a light on the validity of this intuition.

The second term of the gradient in equation 21 maintains the phase rotation and may help the convergence. However, in conducting the numerical tests shown in the next section I have not included this term. The balance between the two terms in the gradient requires a careful implementation of the relative-amplitude response of the linear operators included in equation 21, which is beyond the limitations of my current implementation of these operators.

NUMERICAL EXAMPLES

I conducted some preliminary tests of the theory presented in the previous section. These tests cannot be considered conclusive because of the immature state of the software I am using. In particular, I have not yet included a regularization term in the objective functions that I optimize. Consequently, the iterative estimation did not converge to meaningful results and below I show the results after only three iterations. As explained at the end of the previous section, I also neglected the second term in the expression of the full-gradient in equation 21. Finally, a quasi-Newton optimization scheme should probably be employed to fully benefit from the full-gradient expression in equation 21, whereas I applied a simple conjugate-gradient optimization.

The test dataset is a simple synthetic with two flat reflectors in a constant velocity background. The migration velocity is the correct one (2 km/s) above the shallow reflector and 5% too low betwen the shallow reflector and the deep reflector. Figure 1 shows the prestack migrated cube: the whole cube in panel a), and a zoom around the deep reflector in panel b).

I computed the $\mathbf{\Delta}\rho$ using equation 7 with $\epsilon_{\mathbf{S}} = 0$; that is, I used only the DSO criterion to define a well-focused image. Figure 2 shows the image perturbations computed by applying differential residual-migration operator to the image cube shown in Figure 1: (a) using the gradient expression in equation 14, (b) using the first term of the gradient expression in equation 21. The figure shows the image perturbations before the application of the back-projection operator $\mathbf{L}$ that is at the front of the operator chain in both equation 14 and equation 21. The phases of the two image-perturbation cubes are different. The phase of the cube shown in Figure 2b is similar to the phase of the original migrated cube sown in Figure 1b. In contrast, the image-perturbation cube shown in Figure 2a has a 90 degrees upward phase rotation. This phase rotation may speed up the inversion, as discussed at the end of the previous section.

Figure 3 shows the comparison of the image perturbations computed starting from the image cube shown in Figure 1: and applying: (a) the DSO gradient in equation 22, (b) the differential residual-moveout operator in the first term of the gradient expression in equation 21. Because the velocity error was constant in the horizontal direction, the two image perturbations are similar. They have similar phase and no image perturbations around normal incidence. The inversion of these two image-perturbations cube can thus be expected to produce similar results.

The next three figures show the result of the iterative inversion of the image perturbations shown in Figure 2 and Figure 3a. Figure 4 shows the normalized slowness perturbations computed by the differential residual-migration operator and the gradient expression in equation 14: (a) gradient at first iteration; that is, back-projection of image perturbations shown in Figure 2a: (b) estimation result after three iterations. Similarly, Figure 5 shows the normalized slowness perturbations computed by the differential residual-migration operator and the first term of the gradient expression in equation 21: (a) gradient at first iteration; that is, back-

projection of image perturbations shown in Figure 2b: (b) estimation result after three iterations. Comparing the slowness perturbations shown in Figure 4b with the slowness perturbations shown in Figure 5b, one might conclude that the use of the approximate WEMVA-like gradient might be more stable. However, I do not think that general conclusion can be drawn from this preliminary results.

Finally, Figure 6 shows the normalized slowness perturbations computed by the DSO method: (a) gradient at first iteration; that is, back-projection of image perturbations shown in Figure 3a: (b) estimation result after three iterations. Small differences can be observed between the slowness perturbations after the first and the third iteration. The first three iterations of the conjugate-gradient optimization are mostly spent dealing with the artifacts at the edges of the reflectors, and the erroneous velocity perturbations placed above the shallow reflector by the simple back-projection are not corrected by the following three iterations. This result is also too preliminary to support general conclusions.

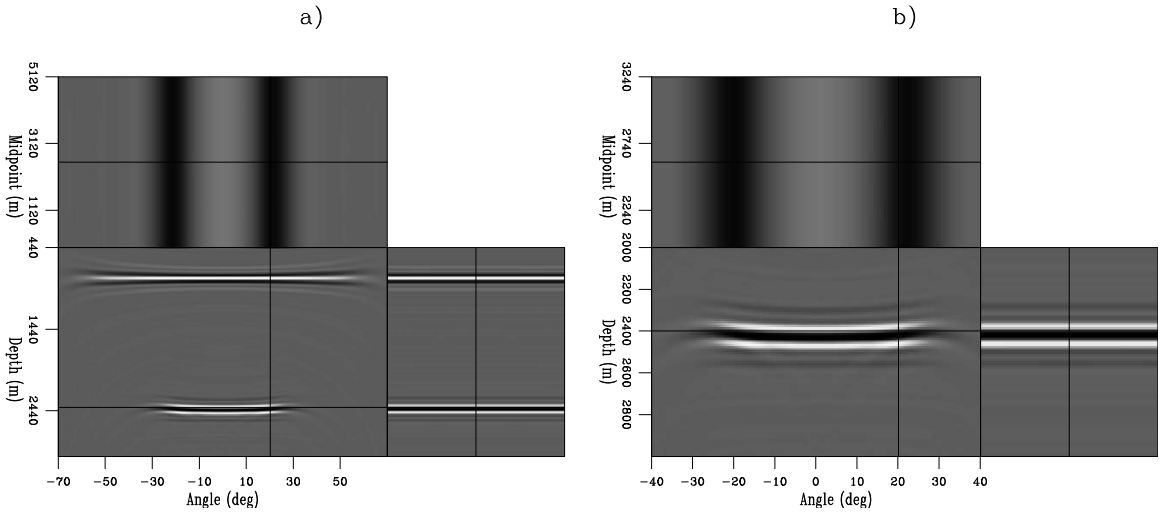

Figure 1: Angle-domain prestack image used to test the velocity-updating process: (a) whole migrated cube, (b) zoom around the deep reflector. The migration velocity model is 5% too low betwen the shallow reflector and the deep reflector. [**CR**]

CONCLUSIONS

I presented a general framework for wave-equation velocity estimation based on the criterion of maximizing the focusing of prestack images after migration, or more precisely, of minimizing the amount of unfocused energy. This framework enabled the definition of an automatic velocity estimation method that benefits from residual migration, but does not require picking residual-migration parameters.

The numerical examples illustrate the basic elements and the concepts underlying the proposed method. They confirm that he method has the potential of updat-

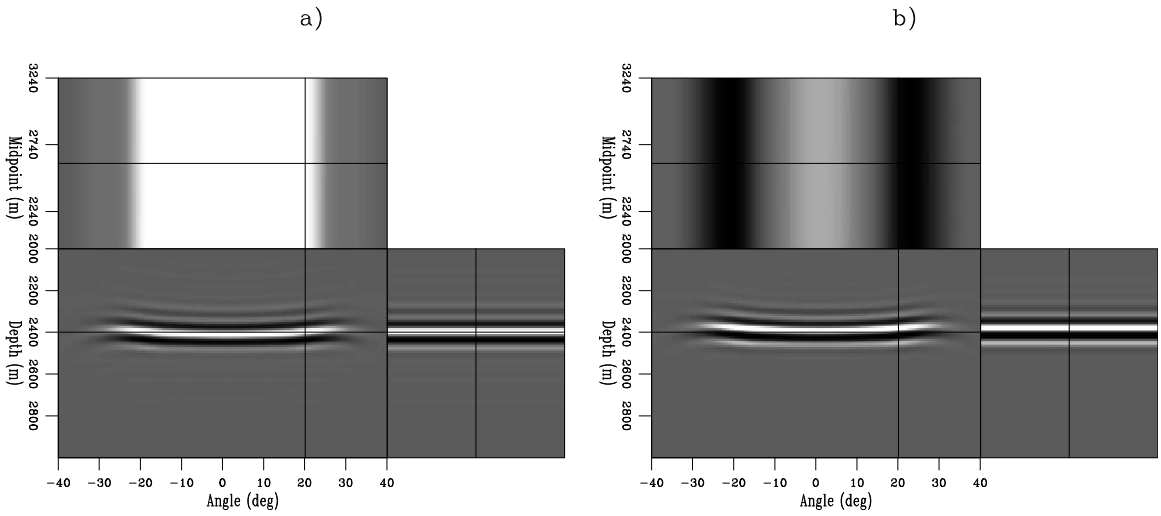

Figure 2: Image perturbations computed by applying differential residual-migration operator to the image cube shown in Figure 1: (a) using the gradient expression in equation 14, (b) using the first term of the gradient expression in equation 21. Notice the phase rotation between the two panels. [**CR**]

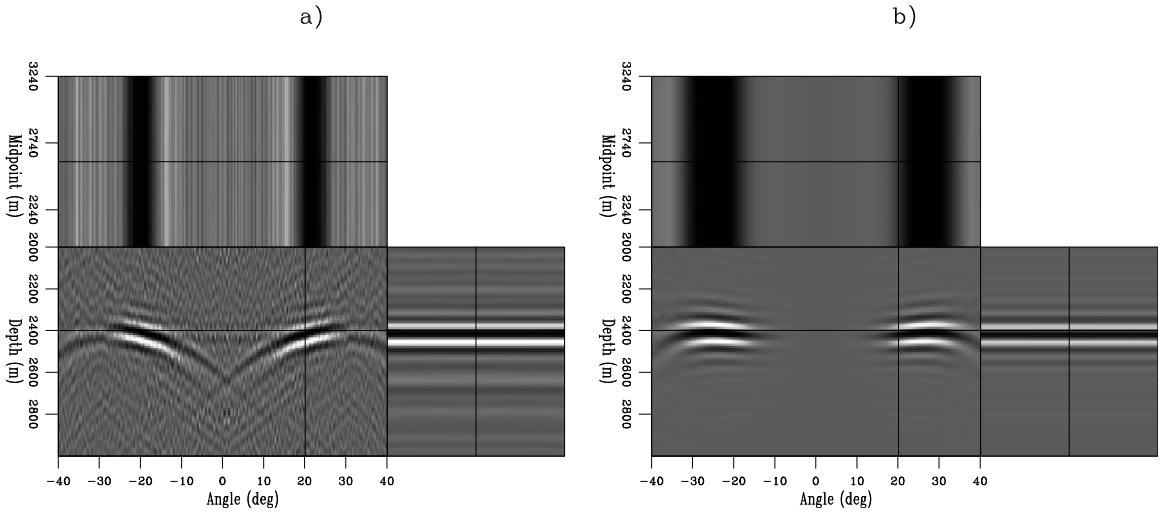

Figure 3: Comparison of the image perturbations computed starting from the image cube shown in Figure 1 and applying: (a) DSO gradient in equation 22, (b) the differential residual-moveout operator in the first term of the gradient expression in equation 21. Notice the similarities. [**CR**]

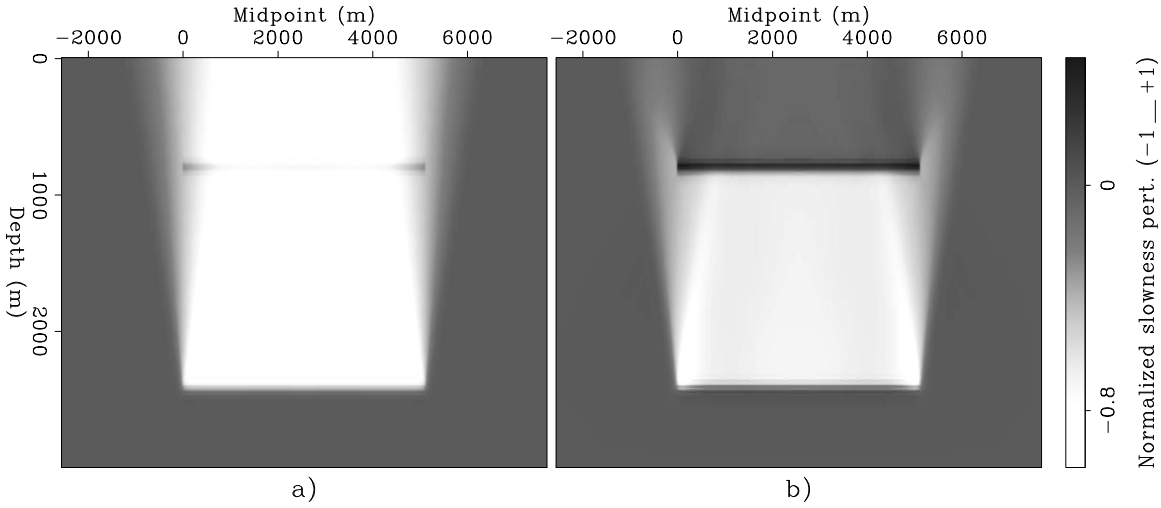

Figure 4: Normalized slowness perturbations computed by the differential residual-migration operator and the gradient expression in equation 14: (a) gradient at first iteration; that is, back-projection of image perturbations shown in Figure 2a, (b) estimation result after three iterations. [**CR**]

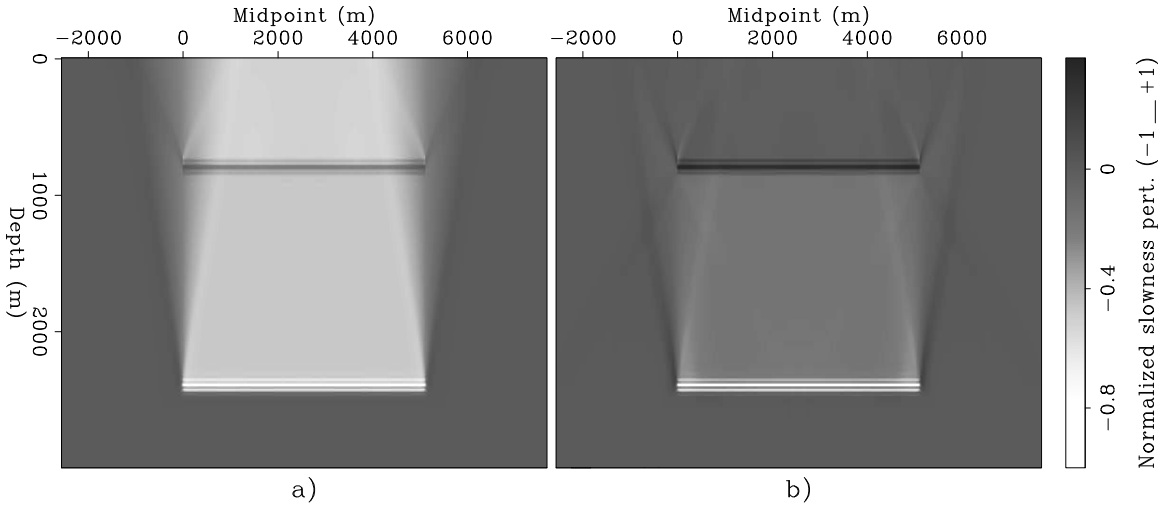

Figure 5: Normalized slowness perturbations computed by the differential residual-migration operator and the first term of the gradient expression in equation 21: (a) gradient at first iteration; that is, back-projection of image perturbations shown in Figure 2b: (b) estimation result after three iterations. [**CR**]

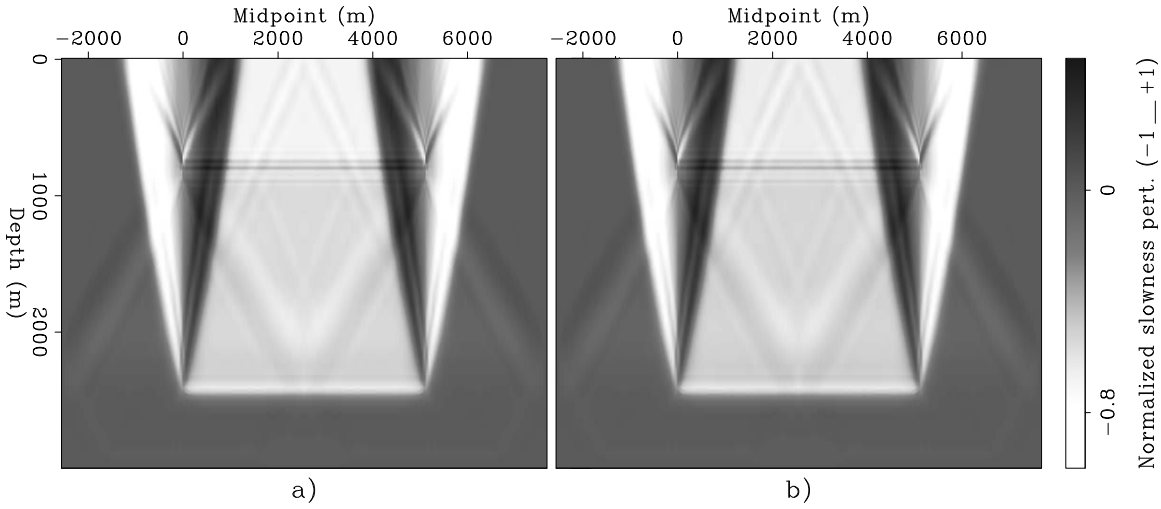

Figure 6: Normalized slowness perturbations computed by the DSO method: (a) gradient at first iteration; that is, back-projection of image perturbations shown in Figure 3a: (b) estimation result after three iterations. [**CR**]

ing the velocity model in the right direction; they are, however, too preliminary to demonstrate its usefulness in practical applications.

APPENDIX A

DIFFERENTIAL RESIDUAL MIGRATION

In this appendix I define the differential residual-migration and residual-moveout operators that are used in the paper, starting from the expression of the residual migration and residual moveout for angle-domain common image gathers introduced in 2D by Biondi and Symes (2004) and in 3D by Biondi and Tisserant (2004). For simplicity, I will derive the operator in 2D, but the 3D extension should be straightforward.

Combining equations D-3 and D-6 in Appendix D of Biondi and Symes (2004), the residual-migration shift $\Delta\mathbf{n}$ along the normal to the reflector $\mathbf{n}$ is given by

$$\Delta\mathbf{n} = -\Delta\rho \frac{\cos\alpha}{\left(\cos^2\alpha - \sin^2\gamma\right)} z_0\mathbf{n} = -\Delta\rho S_{\mathrm{Rmig}}\left(\alpha,\gamma\right) z_0\mathbf{n}, \tag{A-1}$$

where α is the geological dip of the reflector, γ is the aperture angle, and z_0 is the depth of the reflector in the migrated domain with the incorrect velocity. The parameter $\Delta\rho$ depends on the velocity error and is defined as

$$\Delta\rho = \frac{S - S_\rho}{S}, \tag{A-2}$$

where S is the correct migration slowness, and S_ρ is the actual, and incorrect, migration slowness.

If we assume that $\Delta\rho$ is a constant of the spatial coordinates, and ignore the dependency of $\Delta\mathbf{n}$ from the reflector depth z_0 by fixing z_0 at an average value $\bar{z}_0$, the residual migration shift can be applied efficiently in the wavenumber domain, by taking advantage of the well-known relationship between geological dip and the wavenumber:

$$\tan\alpha = \frac{k_x}{k_z}, \tag{A-3}$$

where k_x is the inline midpoint wavenumber and k_z is the depth wavenumber. In the wavenumber domain the residual migration is a simple phase shift linear function of $\Delta\rho$; that is

$$\text{Rmig}\left(\gamma, k_z, k_x\right) = \exp\left[i\Delta\rho S_{\text{Rmig}}\left(k_z, k_x, \gamma\right)\left(k_x \sin\alpha + k_z \cos\alpha\right)\right]. \tag{A-4}$$

To derive the differential residual-migration operator we simply take the derivative of Rmig with respect to $\Delta\rho$. Following the definitions given in the main body we have

$$\mathbf{K}\left[\mathbf{\Delta}\rho\right] = i\Delta\rho S_{\text{Rmig}}\left(k_z, k_x, \gamma\right)\left(k_x \sin\alpha + k_z \cos\alpha\right), \tag{A-5}$$

and

$$\mathbf{M} = iS_{\text{Rmig}}\left(k_z, k_x, \gamma\right)\left(k_x \sin\alpha + k_z \cos\alpha\right)\mathbf{R}\left(k_z, k_x, \gamma\right). \tag{A-6}$$

So far I assumed that $\Delta\rho$ is constant, but in reality we would like to have the parameter $\Delta\rho$ varying, may be smoothly, as a function of the spatial coordinates z and x. That is a potential implementation challenge since I defined the differential residual-migration operator in the wavenumber domain.

For the numerical examples shown in the paper I used the following approximations when applying $\mathbf{K}$ and $\mathbf{M}$ to a spatially varying $\Delta\rho\left(z, x\right)$:

$$\begin{aligned}\mathbf{K}\left[\mathbf{\Delta}\rho\right]\mathbf{R} = \mathbf{M}\left[\mathbf{R}\right]\mathbf{\Delta}\rho = \\ \Delta\rho\left(z, x\right)\mathbf{FFT}^{-1}\left\{iS_{\text{Rmig}}\left(k_z, k_x, \gamma\right)\left(k_x \sin\alpha + k_z \cos\alpha\right)\mathbf{FFT}\left[\mathbf{R}\left(z, x, \gamma\right)\right]\right\},\end{aligned} \tag{A-7}$$

where $\mathbf{FFT}$ and $\mathbf{FFT}^{-1}$ represent forward FFT and inverse FFT, respectively. The error related to this approximation is probably minor when $\Delta\rho\left(z, x\right)$ is a smooth function of the spatial coordinates, since the differential residual-migration operator is a simple differentiator (multiplication by ik_x and ik_z), and thus very compact in the space domain.

In some cases it might be useful to use a differential residual-moveout operator instead of a differential residual-migration operator. A differential residual-moveout

operator can be defined following the same procedure outlined above for differential residual migration, but with the shift function S_{Rrmo} derived from equation D-7 in Appendix D of Biondi and Symes (2004) as

$$S_{\text{Rrmo}}(\alpha,\gamma) = -\frac{\Delta\rho}{\cos\alpha}\frac{\sin^2\gamma}{\left(\cos^2\alpha - \sin^2\gamma\right)}. \tag{A-8}$$

Figure 3 shows an example of the application of equation A-8.

REFERENCES

Albertin, U., P. Sava, J. Etgen, and M. Maharramov, 2006, Adjoint wave-equation velocity analysis: SEG Technical Program Expanded Abstracts, **25**, 3345–3349.

Biondi, B. and P. Sava, 1999, Wave-equation migration velocity analysis: SEG Technical Program Expanded Abstracts, **18**, 1723–1726.

Biondi, B. and W. W. Symes, 2004, Angle-domain common-image gathers for migration velocity analysis by wavefield-continuation imaging: Geophysics, **69**, 1283–1298.

Biondi, B. and T. Tisserant, 2004, 3-D angle-domain common-image gathers for migration velocity analysis: Geophisical Prospecting: accepted for publication, **52**, 575–591.

Maharramov, M. and U. Albertin, 2007, Localized image-difference wave-equation tomography: SEG Technical Program Expanded Abstracts, **27**, 3009–3013.

Sava, P., 2004, Migration and velocity analysis by wavefield extrapolation: PhD thesis, Stanford University.

Sava, P. and B. Biondi, 2004a, Wave-equation migration velocity analysis—I: Theory: Geophysical Prospecting, **52**, 593–623.

———, 2004b, Wave-equation migration velocity analysis—II: Examples: Geophysical Prospecting, **52**, 607–623.

Sava, P. and W. W. Symes, 2002, A generalization of wave-equation migration velocity analysis: SEP-Report, **112**, 27–36.

Sava, P. C., 2003, Prestack residual migration in frequency domain: Geophysics, **68**, 634–640.

Sava, P. C., B. Biondi, and J. Etgen, 2005, Wave-equation migration velocity analysis by focusing diffractions and reflections: Geophysics, **70**, U19–U27.

Shen, P., 2004, Wave equation migration velocity analysis by differential semblance optimization: PhD thesis, Rice University.

Shen, P., E. Menyoli, and H. Calandra, 2005a, Automatic sub-salt velocity analysis: an integrated strategy of ray-based tomography and wave-equation migration velocity inversion: SEG, Expanded Abstracts, **24**, 1978–1980.

Shen, P., W. W. Symes, S. Morton, and H. Calandra, 2005b, Differential semblance velocity analysis via shot profile migration: SEG, Expanded Abstracts, **24**, 2249–2252.

Symes, W. W. and J. J. Carazzone, 1991, Velocity inversion by differential semblance optimization: Geophysics, **56**, 654–663.